Open Access
Archives of Materials Science
Research Article

Hydrogen and Ammonia Gas Sensing Properties of Nanostructured Cobalt Doped Tin Dioxide Based Thick Films at or Near Room Temperature

Sapana Rane[1*], Manish Shinde[2], Sudhir Arbuj[2], Sunit Rane[2], Suresh Gosavi[3]

[1]*Department of Electronics, Mamasaheb Mohol College, Paud Road, Pune, India*
[2]*Centre for Materials for Electronics Technology, Panchawati, Off.Dr. Homi Bhabha Road, Pune-411008, India*
[3]*Department of Physics, Savitribai Phule Pune University, Pune, India*

***Corresponding Author:** Sapana Rane, Department of Electronics, Mamasaheb Mohol College, Paud Road, Pune, India, Tel: +919890968884, E-mail: spna_rane@rediffmail.com

Citation: Sapana Rane (2022) Hydrogen and Ammonia Gas Sensing Properties of Nanostructured Cobalt Doped Tin Dioxide Based Thick Films at or Near Room Temperature. Stechnolock Arch Mater Sci 1: 1-17

ABSTRACT

Cobalt doped tin oxide ($Co_xSn_{1-x}O_2$, where x = 0, 0.01, 0.05 and 0.1) nanoparticles were synthesized by facile solvothermal route at 200 °C for 24 h by varying the doping concentration in order to study their gas sensing performance. Thick films prepared using synthesized nanostructures were studied for their structural, morphological properties and gas sensing performance against different gases. The experimental results revealed that these nanostructured $Co_{0.05}Sn_{0.95}O_2$ and $Co_{0.1}Sn_{0.9}O_2$ films are sensitive to ammonia and hydrogen gas at ambient temperatures of 28°C and 39°C respectively. Thus, depending on the doping concentration, the sensor selectivity can be tuned for ammonia or hydrogen.

Keywords: Thick film; $CoSnO_2$; Sensor; Hydrogen; Ammonia; Gas Sensor

Introduction

Gas sensors based on semiconductor nanostructures have been extensively studied in last couple of decades due to their excellent sensitivities towards different gases, low cost and flexibility in fabrication [1-5]. The requirement of good sensors are high sensitivity and selectivity, fast response and recovery time and lower operation temperature. Many researchers have been tried to make best gas sensor by following the four main strategies viz., i) selecting proper semiconductor oxide material, ii) changing the synthesis methods of existing oxides, iii) making composites with organic semiconductors, carbon nanotubes and graphene iv) utilizing different transition as well as noble metal loading on the semiconductor oxides [6-18]. Apart from this, few reports were also available mentioning the use of different device fabrication approaches viz., inkjet printing, screening printing, direct growth of nanomaterial on chip etc [19- 20]. Among the reported semiconductor oxides, SnO_2 has been one of the most studied oxide material because of its nontoxic, abundant and biocompatible nature [21]. SnO_2 is wide band gap n-type semiconductor and shows excellent changes in the conductivity in presence of reducing as well as oxidising gases. Gas sensing mechanism involves the adsorption of gases on the surface of sensing material and its shows change in the sensor resistance. Means the surface plays important role in governing the response time of sensor. Making the material in nanoform gives higher surface area and also higher reactivity towards the sensing gases. Further, for enhancing the selectivity of the sensing material, the transition metal loading is useful, it selectively adsorbs particular gas at certain temperatures [22-40]. The use of metal oxide loaded on SnO_2 as a gas sensor have also been tried by few researchers [41-43]. *Bai et al* reported the PtCu alloy loaded SnO_2 nanoclusters and showed effective auxiliary detection of diabetic ketosis [44]. Among the available nanomaterial synthesis methods, solvothermal technique provides the nanomaterial having decent properties such as proper size, shape, morphology, crystallinity and surface area. Cobalt oxide is good gas sensing material and being effectively utilized for sensing of many gases owing to its spinel structure where oxygen molecule can be easily adsorbed onto Co_3O_4 surface through oxidation of Co (II) to Co (III) [45-48]. Owing to this, smaller ionic radius than Sn^{4+} ions and exitance of cobalt in two oxidation states, namely Co^{2+} and Co^{3+} makes it convenient as a suitable dopant in SnO_2 based gas sensors.

Observing the importance of SnO_2 and Co_3O_4 as gas sensing materials, here in, cobalt doped SnO_2 nanostructures were synthesized using solvothermal reaction technique and investigated their gas sensing performance towards H_2 and NH_3 gas.

Thick films prepared from synthesized nanostructures revealed that structural, morphological properties and gas sensing performance against different gases such as hydrogen, ethanol and ammonia are dependent on the doping concentration. We believe that this study will open up new possibilities for SnO_2 based economical and solid-state gas sensor fabrication almost at room temperature operation for H_2 and NH_3 gases.

Experimental

Preparation of cobalt doped tin oxide ($Co_xSn_{1-x}O_2$) nanostructured powders

Initially, 10 mmol stannic chloride pentahydrate ($SnCl_4{\cdot}5H_2O$) was dissolved in a beaker containing 50 ml ethylenediamine (EDA) for synthesis of cobalt doped SnO_2 nanoparticles ($Co_xSn_{1-x}O_2$). For doping, Co molar concentration was varied as x = 0, 1, 5, and 10 mole %. While, 'x' mmol of cobaltous chloride hexahydrate ($CoCl_2{\cdot}6H_2O$) was dissolved in 10 mL methanol in another beaker. The solution from second beaker was added to previously prepared stannic chloride solution drop-wise with constant stirring. After 5 min. of homogeneous mixing, this mixture was transferred to a 100 mL stainless steel autoclave with Teflon container. The autoclave was heated in an oven at 200 °C for 24 h after sealing it properly. Afterwards, the autoclave was naturally cooled to room temperature. The obtained material was washed with methanol several times in order to get rid of excess EDA, un-reacted chemicals and reaction by-products. The semi-solid material mass was filtered and dried at 50 °C in vacuum oven.

Physico-chemical characterization

Physico-chemical characterization of the obtained materials was accomplished with different analytical techniques. X-ray diffraction (XRD) study of the prepared powder samples was carried out using Bruker D8 Advance X-ray diffractometer equipped with a monochromator. The instrument employed Ni-filtered CuK_α radiation ($\lambda_\alpha = 1.54$ Å) with 2θ varying from 10° to 80° at a scan speed of 4° min^{-1}. The surface morphological properties of the synthesized powder samples were analyzed under Field Emission Scanning Electron Microscope (FESEM). For this purpose, the dispersion of typical powder sample in ethanol was obtained by mild ultrasonication for 10 min which was drop-cast on 5 x 5 mm aluminum sheet and allowed to dry in air leading to evaporation of ethanol. As a result, thin layer of nanostructured powder was formed on the surface of aluminum sheet. In order to avoid the charging effect, this thin layer was further sputtered with Au and used for FESEM analysis using Hitachi S-4800 field emission scanning electron microscope. Field Emission Transmission Electron Microscopy (FETEM) analysis of the prepared samples (by JEOL JSM-2200FS) was undertaken by drop casting the ethanolic dispersion of the powder on carbon coated TEM grid and subsequent drying in air for few hours.

Fabrication of thick film sensor from nanostructured $Co_xSn_{1-x}O_2$ powders

The synthesized nanostructured $Co_xSn_{1-x}O_2$ powders were used as the functional sensing materials for preparation of thick film gas sensors. First, homogeneous thick film paste was prepared by thoroughly mixing a typical $Co_xSn_{1-x}O_2$ (as functional powder material) and a mixture of 2-2 butoxy-ethoxy ethyl acetate and ethyl cellulose (85-90 % and 10-15 % respectively in appropriate quantities) as an organic binder. Thick films of 1”x1” size was prepared using screen printing technique on glass substrate. The prepared films were then dried under IR lamp (15 minutes) followed by annealing in the muffle furnace (at 400 °C) with dwell time of 1 hour having ramp rate of 2 °C/ min. The thickness of the sensing films was measured using thickness meter and is around 30 μm. Aluminum foil were used as electrode to make contacts on the top of the sensing films. The surface morphological features of the prepared films were observed under scanning electron microscope (SEM, JEOL -JSM-6360A model) by cutting the films into suitable sizes and sputter coating them by a thin gold film.

Figure 1: Gas sensing measurement set up. Inset shows the pictorial view of thick film sensor mounted in the gas sensing measurement system

Gas sensing measurement of $Co_xSn_{1-x}O_2$ thick films

The gas sensing studies of $Co_xSn_{1-x}O_2$ thick films were carried out using the custom-built gas sensing set up consisting of a static gas sensing chamber (having the capacity of 6.3 liter), bridge circuit and data acquisition system as shown in Figure 1. The gas sensing chamber has an in-built heater and electrical contacts station having vacuum creation facility with mixing chamber (inset of Figure 1). The fabricated thick film sensor was positioned in the static gas chamber and its gas sensing behavior was evaluated by measuring the relative change in resistance with and without exposure of gases under consideration. Different gases (e.g., H_2, NH_3 and C_2H_5OH) were used to study the sensing performance of the sensor films. Herein, H_2 was used as in the gaseous form while NH_3 and

C_2H_5OH were used in the form of vapors. Initially, the resistance with respect to temperature of the sensing films was measured. The vapors of NH_3 and C_2H_5OH were prepared by taking a known volume of respective solution in a sealed bottle having rubber cork lid whereas hydrogen gas was used directly in the gas form. The bottle containing the NH_3 or C_2H_5OH was gently heated to 35 to 38 °C and waited for 10 minutes. The formed gas corresponding to the required parts per million (ppm) levels was taken into a calibrated standard plastic syringe and injected into the chamber. After 5 min settling time the change in resistance with respect to temperature was measured. The relative humidity of the test conditions was measured to be 38%. The data was collected using the data acquisition system (DAQ, model-Agilent 34970A, 6 ½ digit). The thick film sensor mounted in the gas sensing measurement system is shown in the inset of Figure 1. Sensor response defined as the R_a/R_g, where R_a is resistance of sensor in air and R_g is the resistance of the sensor in the presence of the analyte gas was calculated from this data.

Results and discussion

XRD analysis of $Co_xSn_{1-x}O_2$ powders

The synthesized Co doped SnO_2 nanostructures prepared by solvothermal reaction technique were characterized using X-ray diffractometry in order to investigate the crystalline phase and purity. Figure 2a depicts the XRD pattern of $Co_xSn_{1-x}O_2$ powder samples where x =0, 0.01, 0.05 and 0.1. Intense yet broad diffraction peaks indicated the generation of highly crystalline nanostructured $Co_xSn_{1-x}O_2$ powders. The reflection peaks at $2\theta = 26.6, 33.9, 37.9, 51.8, 54.7$, and 65.9° can be corroborated with *(hkl)* planes of (110), (101), (200), (211), (220), and (301) respectively for prepared compositions. These diffraction peaks could be easily matched to tetragonal SnO_2 (JCPDS Card File No. 41-1445). The XRD patterns indicated the possibility of Co doping in the SnO_2 lattice for the doped samples which is obvious considering the ionic radius of Co^{2+}(0.72Å) which is closer to ionic radius of Sn^{4+} (0.71 Å). Additionally, any extra peaks related to CoO, Co_2O_3 could not be observed which confirmed the substitution of Co ions in place of Sn. The average grain size of $Co_xSn_{1-x}O_2$ nanostructures calculated using *Scherrer's* formula ($D=0.9\lambda/\beta\cos\theta$, where D is crystallite size, λ is the wavelength of applied X-ray,θ is the diffraction angle and β is the full width at half maximum (FWHM) of the diffraction peak) was found to be in the range of 5 to 7 nm. The data of *hkl* planes and average crystallite (grain) size of $Co_xSn_{1-x}O_2$ nanostructures calculated using *Scherrer's* formula was tabulated in Table 1.

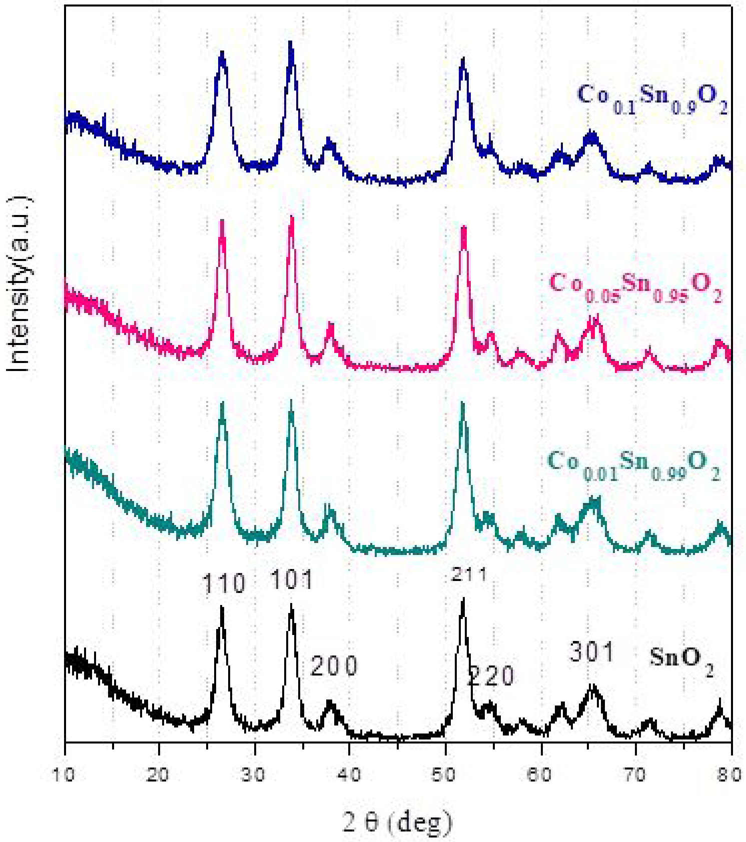

Figure 2: X-ray diffractogram of nanostructured $Co_xSn_{1-x}O_2$ powders

Material	(*hkl*)	FWHM (deg.)	2Θ	Crystallite size (nm)	Average crystallite (nm)
SnO_2	(110)	1.3533	26.52	6.036	6.32
	(101)	1.2584	33.84	6.606	
$Co_{0.01}Sn_{0.99}O_2$	(110)	1.4354	26.57	5.691	6.08
	(101)	1.2821	33.84	6.482	
$Co_{0.05}Sn_{0.95}O_2$	(110)	1.2920	26.56	6.322	6.76
	(101)	1.1541	33.84	7.203	
$Co_{0.1}Sn_{0.9}O_2$	(110)	1.7729	26.57	4.607	5.09

Table 1: Data of *hkl* planes and average crystallite size of $Co_xSn_{1-x}O_2$ nanostructures

Surface morphological analysis of $Co_xSn_{1-x}O_2$ powders

Figure 3 showed the FESEM images of the synthesized powder samples. From the FESEM analysis, uniform formation of spherical nanoparticles with size around 10 nm was seen in case of pure SnO_2 sample (Figure 3a). A trend of reduction in particle size due to increase of Co loading was observed in Figure 3b-d. The formation of mono-dispersed spherical nanoparticles having size in the range of 4 to 5 nm were observed in case of $Co_{0.01}Sn_{0.9}O_2$, $Co_{0.05}Sn_{0.95}O_2$ and $Co_{0.1}Sn_{0.9}O_2$ samples (Figure 3 c,d).

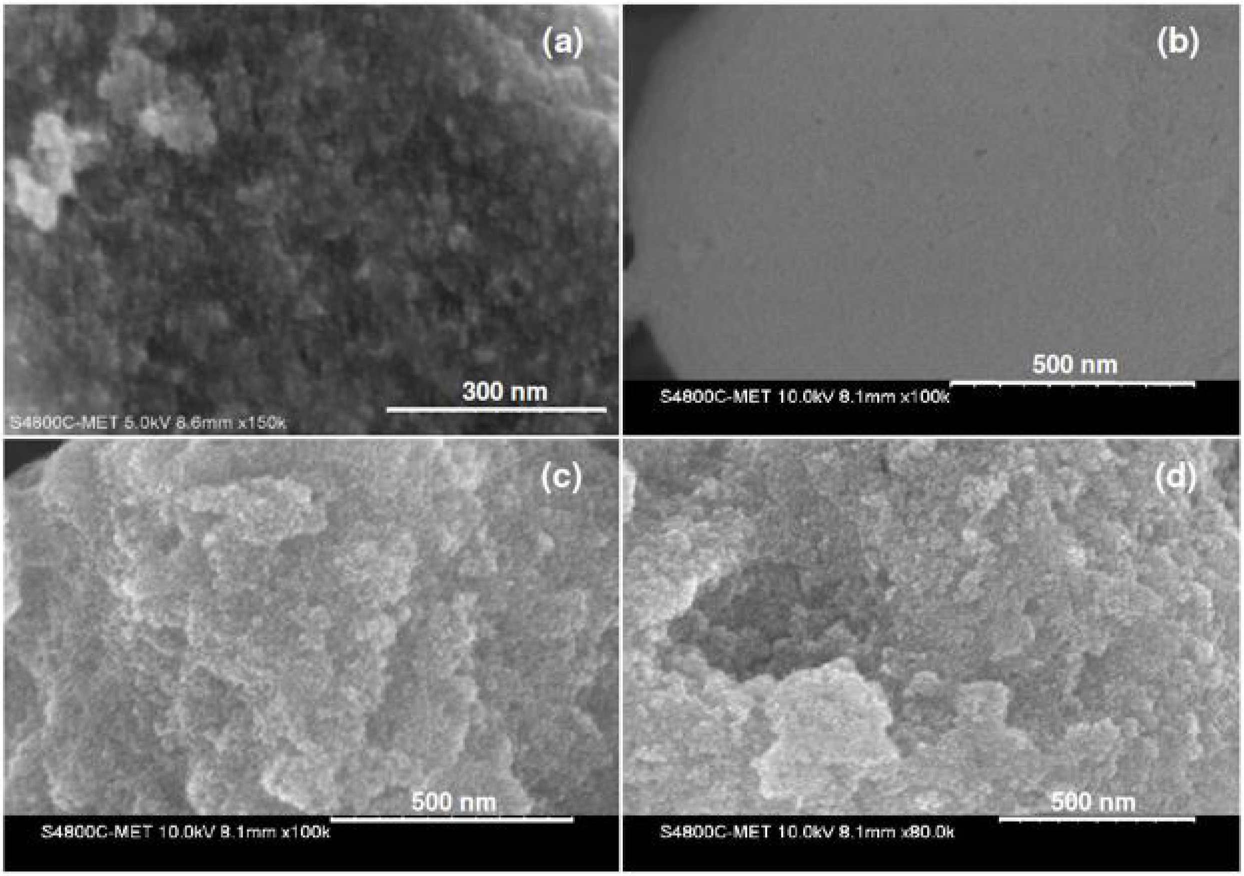

Figure 3: FESEM images of $Co_xSn_{1-x}O_2$ nanostructures where x is (a) 0, (b) 0.01, (c) 0.05 and (d) 0.1

FETEM analysis of $Co_xSn_{1-x}O_2$ nanostructures

Figure 4 showed the representative FETEM images of $Co_{0.05}Sn_{0.95}O_2$ sample synthesized with Co doping of 5 mol %. These images displayed nanostructures having particles size in the range of 5-20 nm with spherical and elongated rod like morphology (Figure 4a, b). The length of nanorods varied in the range of 10-20 nm while the width varied from 5 nm to 10 nm. High resolution TEM image (Figure 4c) exhibited nano-crystallites having orientation in different directions as represented by different coloured lines corresponding to different crystalline planes. Slight increase in lattice parameters was noted which can be attributable to the Co doping. The SAED pattern shown in the Figure 4d indicated the formation of highly crystalline $Co_{0.05}Sn_{0.95}O_2$ and the consequent d-values matched well with the XRD data of the corresponding sample.

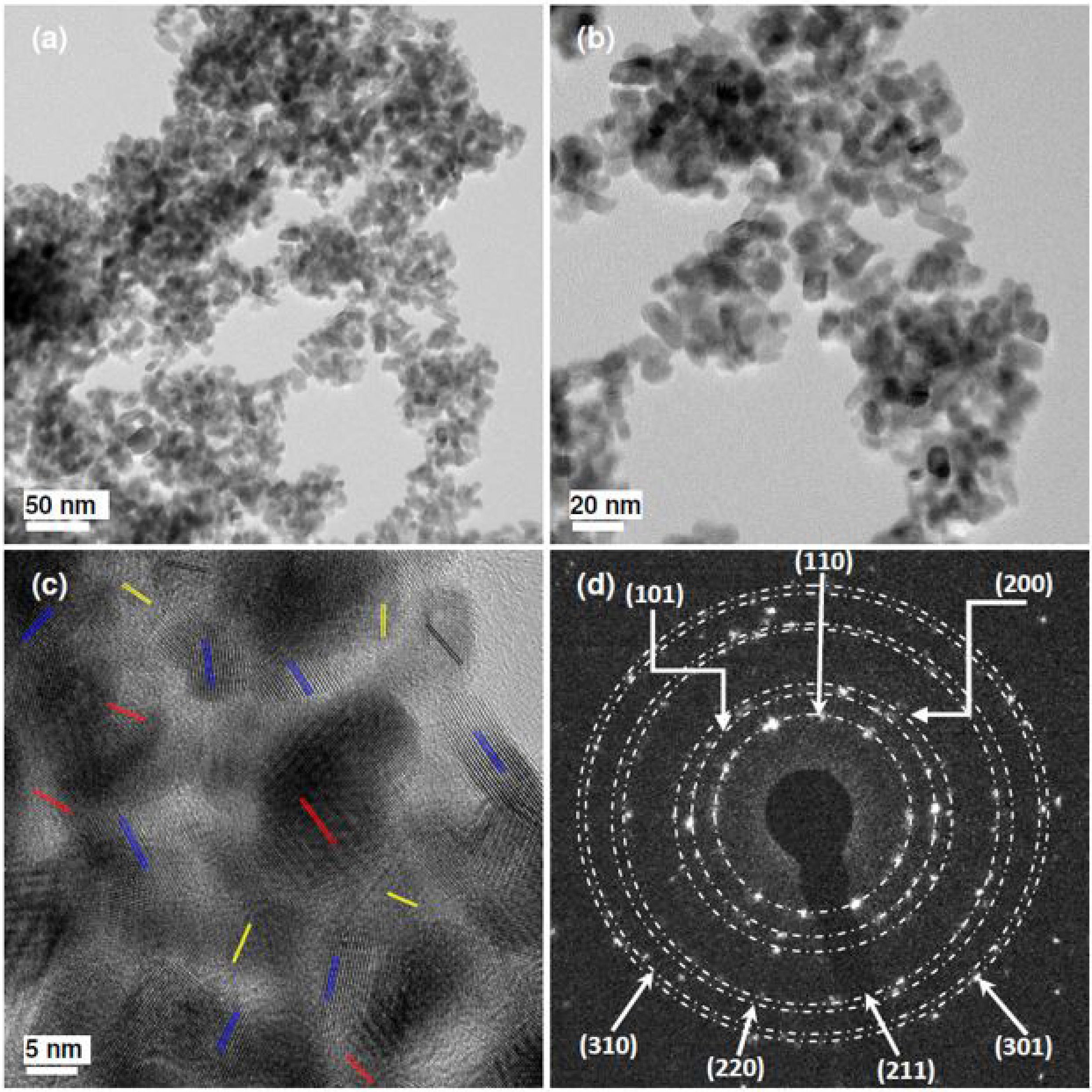

Figure 4: FETEM images of $Co_{0.05}Sn_{0.95}O_2$nanostructures: (a) low magnification, (b) intermediate magnification, (c) lattice image (blue, red, black and yellow colors correspond to (110), (101), (200) and (211) crystalline planes respectively) and (d) SAED pattern

XPS analysis of $Co_{0.05}Sn_{0.95}O_2$ nanostructures

The elemental composition and oxidation states of 5% Co-doped SnO_2 nanopowder was determined by X-ray photoelectron spectroscopy (XPS) and the spectra are shown in Figure 5. General identification of elements present in the sample was accomplished by the XPS survey spectra which provided the corresponding elemental compositions (Figure 5a). It can be seen that all anticipated elements were detected (Sn, O and Co), however, the peak corresponding to Co is very low in intensity. Tin core levels, namely, Sn $3d_{5/2}$ and Sn $3d_{3/2}$ which are shown in Figure 5b (at high resolution scan) were found to be composed each of the main peak and a minor peak at lower and higher binding energy respectively, which pointed to the presence of Sn species possessing two different oxidation states [49]. The presence of higher intensity peaks at the binding energies of 486.7 eV and 495.3 eV and their binding energy difference of 8.6 eV were attributed to Sn^{4+} state of SnO_2 [40, 50]. The low intensity peaks at 487.4 eV and 495.7 eV were ascribed to Sn^{4+} of $Sn(OH)_4$ [51]. In the case of Co, the absence of XPS peak at 778.2 eV corresponding to Co metal and presence of peak around 780.3 eV due to Co 2p in high resolution spectra scan (Figure 5c) affirms that the Co is in the ionic form in Co-SnO_2 samples [52]. By noting the two distinct peaks in Figure 5c at 780.3 eV ($2p_{3/2}$) and 796.2 eV ($2p_{5/2}$), the chemical state of Co is inferred to be +2. Moreover, the binding energy difference of 15.9 eV and presence of satellite peaks at 786.2 and 803.1 eV rule out the presence of Co^{3+}. [26, 49, 51, 53-54]. Nearly equal ionic radii corresponding to Co^{2+} (0.72 Å) and Sn^{4+} (0.71 Å) suggested that substitutional type dopant loading occurs which might lead to creation of oxygen ion vacancies [38]. The high-resolution survey scan corresponding to O 1s peak (Figure 5d) at 530.0 eV asserted that oxygen existed in the normal chemical state -2 in the lattice, while, the minor peak at 532.4 eV was assigned to the chemisorbed oxygen species O^{2-}, O^{-}, etc. [40, 50].

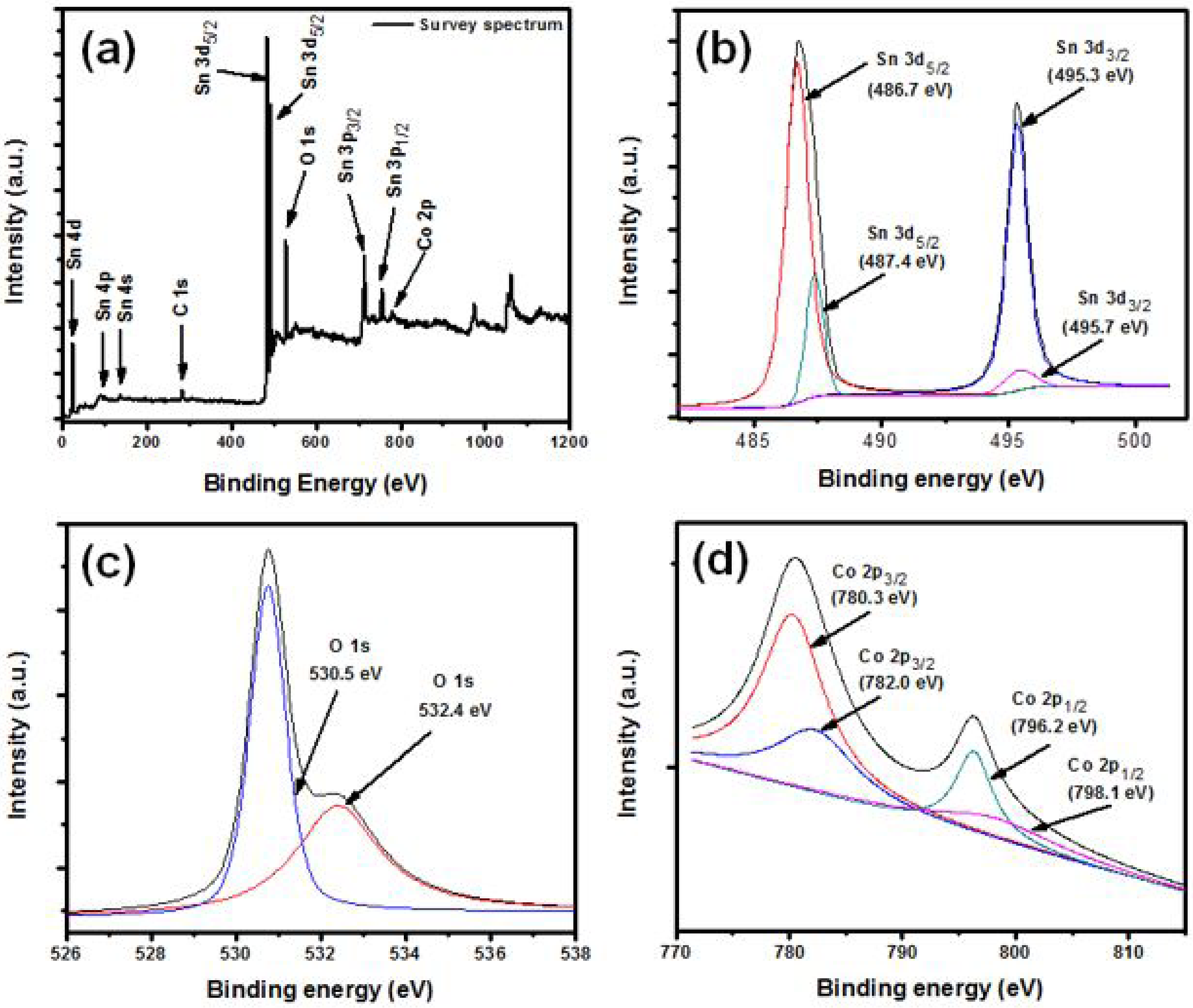

Figure 5: XPS spectra of 5% Co-doped SnO_2: (a) survey spectra and high resolution XPS core-level spectra corresponding to (b) Sn 3d, (c) Co 2p and (d) O 1s

Sample	H_2 (150 ppm)		NH_3 (150 ppm)		Ethanol (150 ppm)	
	Op. temp. (°C)	Response	Op. temp. (°C)	Response	Op. temp. (°C)	Response
SnO_2	201	4.48	165	1.40	255	4.35
$Co_{0.01}Sn_{0.99}O_2$	80	1.25	64	0.73	210	2.15
$Co_{0.05}Sn_{0.95}O_2$	43	0.13	28	10.7	166	1.30
$Co_{0.1}Sn_{0.9}O_2$	39	1.78	52	1.53	84	0.46

Table 2: Gas sensor response and operating temperature of pure and Co doped SnO_2 films corresponding to H_2, NH_3 and ethanol

Surface morphology studies of $Co_xSn_{1-x}O_2$ thick films

The surface morphological aspects of the sensing films was detected under SEM as shown in Figure 6. The particles were seen to be connected to each other forming void free surface in case of all samples. The increase in the particle size for all the samples is quite obvious due to annealing of the films at 400 °C for 60 min. Similar to the case of powder samples, the film based on pure SnO_2 powder showed larger size of particles (Figure 6a) than that of the doped samples (Figure 6b-d). The powders prepared using increased doping concentrations exhibited more uniform surface morphologies of the films. Energy dispersive analysis (EDS) investigation asserted the presence of Co (Figure 6e and its inset).

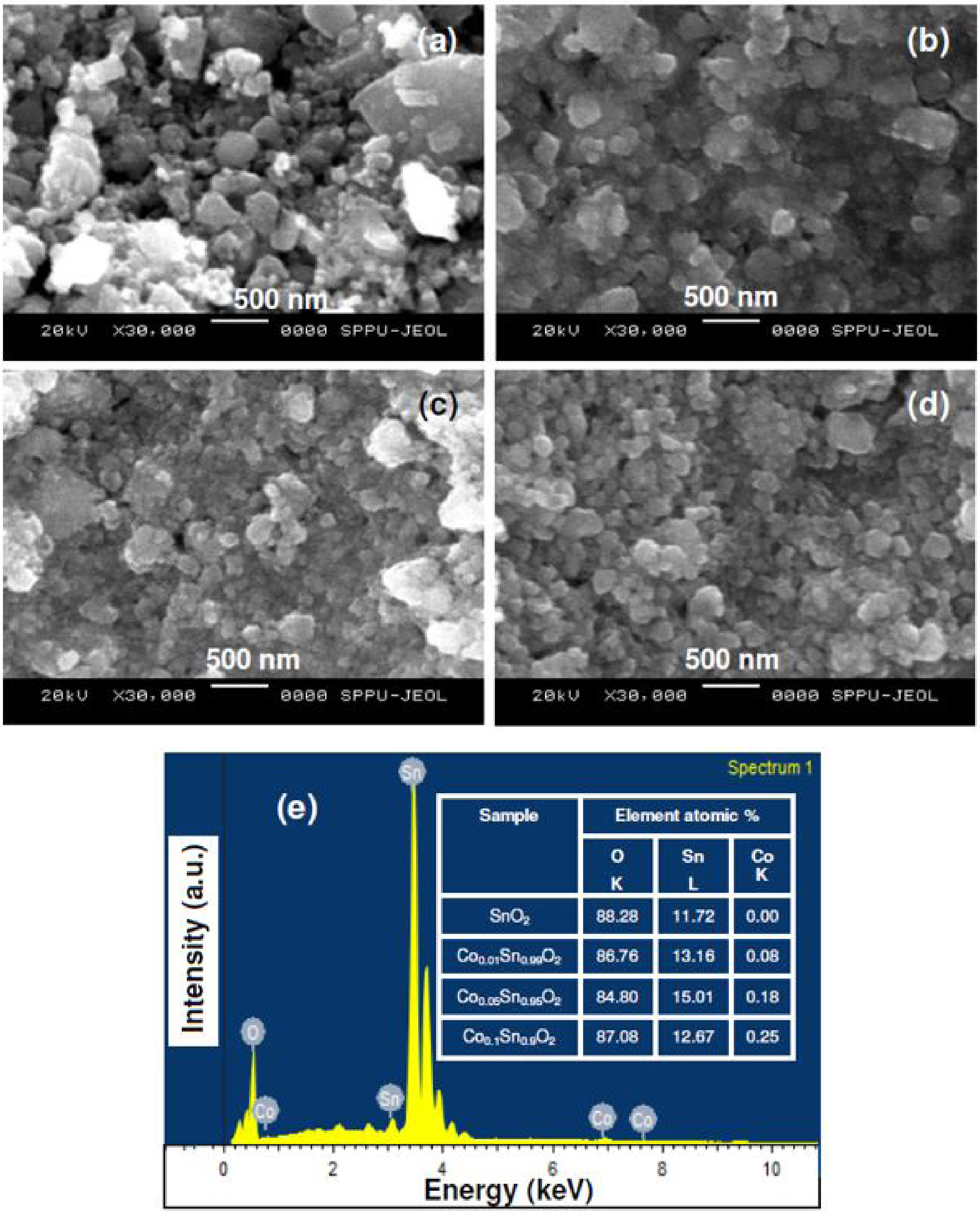

Sample	Element atomic %		
	O K	Sn L	Co K
SnO_2	88.28	11.72	0.00
$Co_{0.01}Sn_{0.99}O_2$	86.76	13.16	0.08
$Co_{0.05}Sn_{0.95}O_2$	84.80	15.01	0.18
$Co_{0.1}Sn_{0.9}O_2$	87.08	12.67	0.25

Figure 6: FESEM analysis of thick film prepared using $Co_xSn_{1-x}O_2$ nanostructures where x is (a) 0, (b) 0.01, (c) 0.05 and (d) 0.1, while (e) Typical EDS spectrum of $Co_xSn_{1-x}O_2$ thick films. Inset of Fig. 6e showed table of elemental compositions of different samples

Sensor response to various gases

Figure 7a exhibited the response of the $Co_xSn_{1-x}O_2$ films (x= 0, 0.01, 0.05 and 0.1) based sensor to H_2 gas. It was observed that the gas sensor fabricated using pure SnO_2 powder showed the optimum operating temperature of 110°C with sensor response of 4.48 at 150 ppm concentration. This optimum operating temperature was drastically reduced due to the doping of Co to 80 °C for $Co_{0.01}Sn_{0.99}O_2$, 43 ºC for $Co_{0.05}Sn_{0.95}O_2$ and 39 ºC for $Co_{0.1}Sn_{0.90}O_2$ with the sensor response (R_a/R_g) of 1.25, 0.127 and 1.78 respectively. Additionally, the gas sensor based on 1 mol% Co doped SnO_2 sample ($Co_{0.01}Sn_{0.99}O_2$) showed increase in sensor response to 1.28 around at 165 °C which further increased to 1.7 at 236 °C. From the results, it can be said that the cobalt doping is responsible to lowering the optimum operating temperature of the sensor. For H_2 gas, the thick film sensors with 10 % Co doping into SnO_2 exhibited the operating temperature of 39 °C which is very close to room temperature. The sensor response to NH_3 and ethanol gases was also studied and the results are shown in Figure 7b and Figure 7c respectively. These Figures revealed that as the cobalt doping increased into SnO_2 matrix, the operating temperature of the sensor decreased for both NH_3 and ethanol gas. The $Co_{0.05}Sn_{0.95}O_2$ sensor (5 mol% Co doping) showed a room temperature operation (28 °C) with the highest sensor response of 10.7 for NH_3 gas (Figure 7b). On the other hand, ethanol thick film sensor based on $Co_{0.1}Sn_{0.9}O_2$ nanopowder exhibited least operating temperature of 84 °C with response of 0.84 (Figure 7c). For ethanol sensing, the response also decreased with respect to the operating temperature. The reproducibility and repeatability analysis of each type of sensor was performed for 3 samples and ±5% variation was observed. Only the representative data was shown in Figure 7.

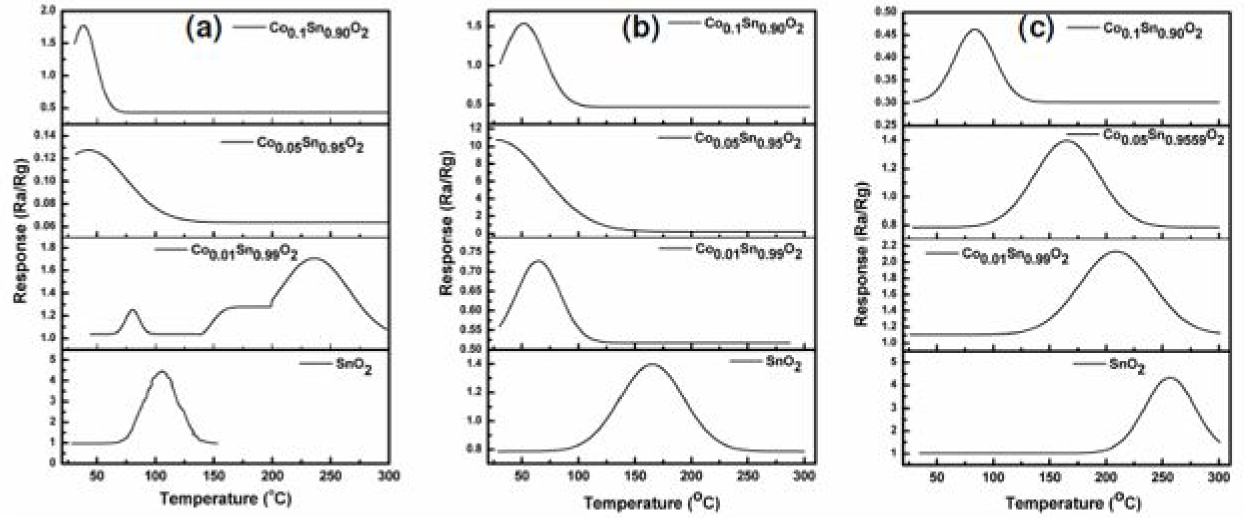

Figure 7: Sensor response with respect to temperature of $Co_xSn_{1-x}O_2$ films (where x = 0, 0.01, 0.05 and 0.1) at concentration of 150 ppm for (a) H_2 gas, (b) NH_3 vapor and (c) ethanol vapor

Table 2 showed the tabulated data of the sensor response (R_a/R_g) and operating time corresponding to H_2, NH_3 and ethanol gases for thick film gas sensor based on $Co_xSn_{1-x}O_2$ nanopowders. The comparison of gas sensing performance in terms of response and operating temperature for the present $Co_xSn_{1-x}O_2$ thick films based gas sensors with already reported Co-doped SnO_2 based gas sensors is provided in Table 3. The comparison revealed that though, the response of these sensors is better than the present work, the operating temperature and concentration of analyte gas (in ppm) were at higher side in most of the reported cases. Based on the obtained results, we can say that the presented gas sensors are better and favorable than that of the reported ones considering at or near room temperature operation and low gas concentration.

The change in sensor response with respect to the analyte gas concentration was studied only for the H_2 gas and NH_3 vapor for $Co_{0.1}Sn_{0.90}O_2$ and $Co_{0.05}Sn_{0.90}O_2$ thick films based gas sensors respectively at their corresponding operating temperatures as the operating temperatures for H_2 gas and NH_3 vapors were obtained to be 39ºC and 28 ºC as compared to ethanol vapor. The sensor response for different concentrations of NH_3 gas observed up to 1050 ppm at the operating temperature of 28°C for $Co_{0.05}Sn_{0.95}O_2$ thick films based gas sensor showed linear change with respect to change in concentration of NH_3 gas as exhibited in Figure 8a. Similar study on the sensor response for different concentrations of H_2 gas was carried out up to 1050 ppm at the operating temperature of 39 °C for $Co_{0.1}Sn_{0.90}O_2$ thick films based gas sensor (Figure 8b). However, the linear change with respect to change in concentration of H_2 gas is not very consistent as compared to NH_3 gas as inferred from the fact that the correlative coefficient (R^2) values (as shown in tables in the inset of the respective figures) were found to be 0.7978 and 0.9846 respectively [55-56]. The sensor response for different gases at various operating temperatures has been represented in Figure 9. It can be inferred from the graph that the best response has been obtained from the $Co_{0.05}Sn_{0.95}O_2$ gas sensor for NH_3 gas at an operating temperature of 28 °C.

The response and recovery of the sensor were also measured for H_2 and NH_3 gas. The sensor showed the response and recovery time of 10 s and 110 s respectively for H_2 gas whereas for NH_3 it was 10 s and 150 s respectively.

Sr. No.	Co doped SnO_2	Synthesis method	Analyte gas	Operating temperature [°C]	Concentration [ppm]	Response [R_a/R_g]	Response/ recovery time	Ref
1.	Nano-fibres	Electro-spinning	Methane	300	50	30	15 s/12 s	[16]
2.	2 at. %, Thin film (160 nm thickness)	RF magnetron sputtering	Sarin and yperite	210	25-50	--	--	[20]
3.	1-5 mol % Co Nano-fibres	Electro-spinning	VOCs	300	100 (ethanol)	40	--	[21]
4.	0.5-3 wt %, Nanoparticles	Co-precipitation	Ethanol	250	2000	120	3 s/15 s	[28]
5.	0.5-3 at % Nanoparticles	Co-precipitation	Hydrogen	--	500	4	--	[29]
6.	Graphene supported Nanoparticles	Flame spray pyrolysis	Ethanol	350	1000	2147	1 s/--	[30]
7.	0.5-3 wt %, Nano-fibres	Electro-spinning	Hydrogen	330	100	24	2 s/3 s	[22]
8.	10 mol %, Nanoparticles	Solvothermal	Hydrogen	39	150	1.78	10 s/110 s	Present work
9.	5 mol %, Nanoparticles	Solvothermal	Ammonia	28	150	10.7	10 s/150 s	Present work

Table 3: Comparison of sensor properties achieved in the present work with available literature reports

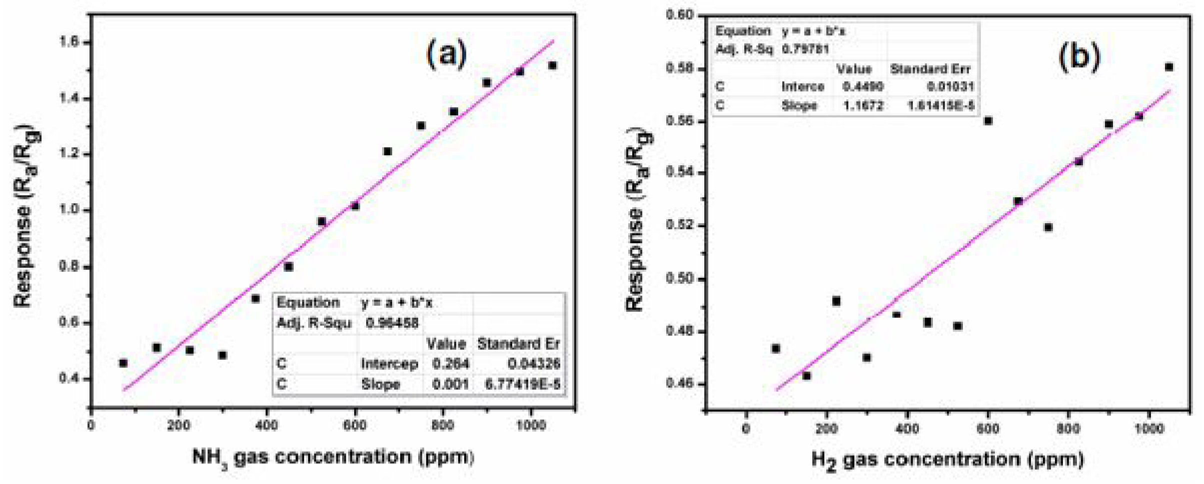

Figure 8: Sensor response to (a) NH_3 vapors of different concentrations (ppm) for $Co_{0.05}Sn_{0.95}O_2$ thick films at 28°C and (b) H_2 gas of different concentrations (ppm) for $Co_{0.10}Sn_{0.90}O_2$ thick films at 39°C

Mechanism of gas sensing

Transition metals such as Co, Ni, etc. are recently being explored as dopants, which act as activating catalyst to accelerate the chemical reaction process and consequently improve the gas sensor performance [57-60]. As the most used semiconductor gas sensing material, SnO_2 possesses typical n-type nature. The gas sensing mechanism of SnO_2 is explained so far using various models. The most widely accepted model states that its sensing properties are predominated by the change of SnO_2 surface resistance, especially the adsorption and desorption of oxygen on the surface of sensing materials [61-62]. When SnO_2 nanoparticles are exposed to air, oxygen adsorbs on their exposed surface and ionizes to O^- or O_2^- (O^- is considered to be dominant), which results in a decrease of the carrier concentration and electron mobility [32, 63]. The decrease in the charge carrier concentration in the conduction band results in the formation of the electron depletion layer on the surface of SnO_2 nano-grains and upward band bending at grain boundaries. Such potential barrier at grain boundaries increases resistance due to restriction to the flow of electrons [31, 64].

Doping of transition metals such as cobalt could effectively suppress grain growth of SnO_2, creating more sensitive sites on the grain boundaries exposing to target gas and can be advantageous for improvement in sensitivity of gas sensor [27, 31]. Smaller ionic radius and valence of Co^{2+} (0.58 Å) than Sn^{4+} (0.69 Å) can lead to Co ions getting substituted at Sn^{4+} site in SnO_2 [65]. Such substitution would also decrease the grain size of SnO_2. Based on solid-state chemistry theory, relatively higher concentration of surface oxygen vacancies can be formed due to Co ions substitution in the Co-doped SnO_2 nanoparticles, which will trap larger number of free electrons (adsorption of oxygen species on the surface of the doped SnO_2 nanoparticles), which in turn, would intensely affect the gas sensor response [31, 66-67]. The reducing gas like H_2, upon exposure to the sensing material during gas sensing, interacts with the adsorbed oxygen molecules and release of trapped electrons back to the conduction band takes place. This increases the carrier concentration as well as mobility of SnO_2 leading to the decrease in resistance. For Co doped SnO_2 based gas sensors, the response varied for different gases and maximum being for NH_3 gas for sample prepared with 5 mol % doping. However, improvement in response for ethanol due the doping of Co was not observed. These changes in the response are ascribable to the changes in the barrier height which arise because of doping change and depend on the gas. However, this may also provide the selectivity to a particular gas by effectively changing the doping concentration which was noted as shown in Figure 7. Strangely, in case of gases like H_2, NH_3 and ethanol, the sensor response was <1, implying the increase in the resistance upon exposure to gas at 5%, 1% and 10 % doping concentration (Figure 8). Similarly, at least operating temperature, the sensor response was <1 for 100-1000 ppm in case of H_2 gas (at 10 mol% Co-doping concentration) and up to 500 ppm concentration for NH_3 gas (at 5 mol% Co-doping concentration) respectively. It has been reported that heavy doping greater than 2-4 % can exert negative influence on some of the gas sensing properties [68]. In the present case, better selectivity and lower operating temperature was obtained, however, the sensor response was reduced (even <1 in some cases). It has been reported that surface disorder introduced by doping may be exclusively accompanied by enhancement of the surface state density which could cause pinning of surface Fermi level and subsequent increase of resistance [69-70]. Such increased resistance may be the reason for the sensor response <1 in certain cases. In particular case of NH_3 gas, up to 500 pm the sensor response was noted to be <1 up to 500 ppm, however, the response improved and was found to be >1 above 500 ppm which may be attributed to occupation of surface state density sites more number of adsorbed gas molecules and subsequent decrease of resistance.

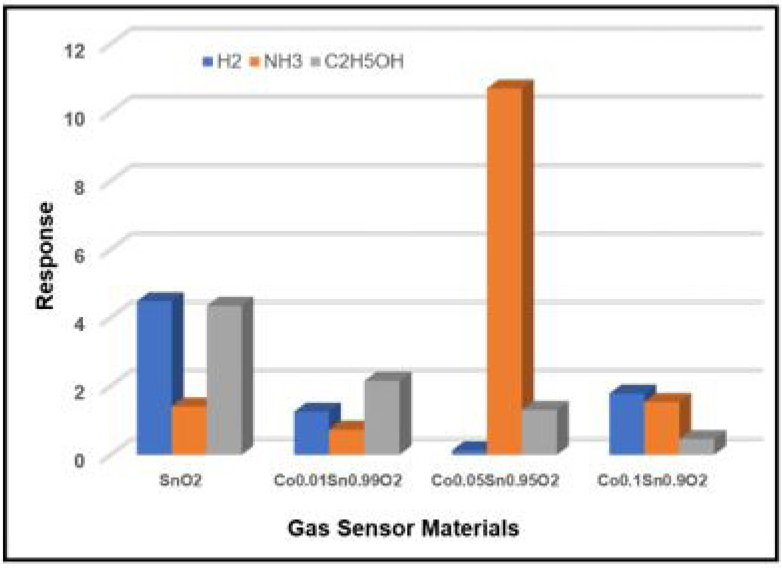

Figure 9: Sensor response of $Co_xSn_{1-x}O_2$ films for different gases at various operating temperatures

Conclusion

Cobalt doped tin oxide nanoparticles ($Co_xSn_{1-x}O_2$, where x= 0, 0.01, 0.05 and 0.1) were synthesized using facile solvothermal technique at 200°C. The analytical studies using physico-chemical characterization techniques exhibited generation of pure as well as Co doped SnO_2nanostructures. Nanostructured pure SnO_2 and Co doped SnO_2 powders based thick film sensors (resistive type) were prepared and subsequently characterized by physical and electrical methods. The fabricated nanostructured films based sensors disclosed sensitivity to different gases such as hydrogen, ammonia and ethanol with low operating temperature in the range of 28°C to 256 °C which was found to be dependent on the amount of Co doping in SnO_2 nanoparticles and the test gas. In case of ammonia gas the operating temperature was 28 °C (for 5mol % Co-doped SnO_2), while for hydrogen gas it was close to 39 °C (for 10 mol % Co-doped SnO_2), and for ethanol gas vapor detection it was 84 °C (for 10 mol % Co-doped SnO_2). Thus, the highest sensitivity of the prepared films towards NH_3 gas was observed at room temperature followed by hydrogen (H_2) gas near room temperature. The response and recovery of the sensor were also measured for H_2 and NH_3 gas. The response and recovery time of Co doped SnO_2 sensor for H_2 gas was 10 s and 110 s respectively whereas for NH_3 it was 10 sec and 150 s respectively. From the above results it can be concluded that the nanostructured $M_xSn_{1-x}O_2$ (M = Co, Ni, Zn, etc.) films would be promising candidates towards the reduction of operating temperature of the gas sensors by varying transition metal and its doping concentration.

Acknowledgments

One of the authors, Dr. Sapana Rane is grateful to Director, C-MET, Pune for granting permission to carry out the experimental work, Shri. Shinde, Department of Physics, SPPU, Pune for providing the SEM images. She is also grateful to Pune District Education Association, Pune.

References

1. M. Prudenziati (1994) 'Thick Film Sensors' Handbook of Sensors and Actuators, Elsevier Science, Amsterdam, The Netherlands 1: 1-10.

2. SF Bamsaoud, SB Rane, RN Karekar, RC Aiyer (2011) Nano particulate SnO2 based resistive films as a hydrogen and acetone vapour sensor, Sens. Actuat. B: Chem 153: 382.

3. SS Rane, S Tatkare, SB Rane, SW Gosavi (2012) Thick Film Hydrogen sensor based on nanocrystalline nickel ferrite prepared using simple microwave oven, IEEE explore, Proc., 1st International Symposium on Physics and Technology of Sensors (ISPTS-1) 2012: 212-5.

4. SF Bamsaoud, SB Rane, RN Karekar, RC Aiyer (2012) SnO2 film with bimodal distribution of nano-particles for low concentration hydrogen sensor: effect of firing temperature on sensing properties, Mat Chem Phys 133: 681-7.

5. SF Bamsaoud, SB Rane, RN Karekar, RC Aiyer (2010) Naosize SnO2 based tubular resistive gas sensor for hydrogen and acetone vapour, Trans. Ind Ceram Soc 69: 193-7.

6. N Kaur, M Singh, E Comini (2020) One-Dimensional Nanostructured Oxide Chemoresistive Sensors, Langmuir 36: 6326–44.

7. A Rao, H Long, AH Trochimczyk, T Pham, A Zettl, C Carraro, R Maboudian (2017) In Situ Localized Growth of Ordered Metal Oxide Hollow Sphere Array on Microheater Platform for Sensitive, Ultra-Fast Gas Sensing, ACS Appl Mater. Interf 9: 2634-41.

8. HW Kim, HG Na, YJ Kwon, SY Kang, MS Choi, et al. (2017) Microwave-Assisted Synthesis of Graphene–SnO2 Nanocomposites and Their Applications in Gas Sensors, ACS Applied Mater Interf 9: 31667-82.

9. JH Lee, A Katoch, SW Choi, JH Kim, HW Kim, SS Kim (2015) Extraordinary Improvement of Gas-Sensing Performances in SnO2 Nanofibers Due to Creation of Local p–n Heterojunctions by Loading Reduced Graphene Oxide Nanosheets, ACS Appl Mater Interf 7: 3101-9.

10. H Liu, W Zhang, H Yu, L Gao, Z Song, S Xu, et al. (2016) Solution-Processed Gas Sensors Employing SnO2 Quantum Dot/ MWCNT Nanocomposites, ACS Appl. Mater. Interf 8: 840-6.

11. Y Yang, S Li, W Yang, W Yuan, J Xu, Y Jiang (2014) In Situ Polymerization Deposition of Porous Conducting Polymer on Reduced Graphene Oxide for Gas Sensor, ACS Appl. Mater. Interf 6: 13807-14.

12. R Arora, U Mandal, P Sharma, A Srivastav (2017) Nano composite film Based on Conducting Polymer, SnO2 and PVA, Materials Today: Proceedings 4: 2733-8.

13. Z Song, J Yan, J Lian, W Pu, L Jing, et al. (2020) Graphene Oxide-Loaded SnO2 Quantum Wires with Sub-4 Nanometer Diameters for Low-Temperature H2S Gas Sensing, ACS Appl. Nano Mater. 3: 6385-93.

14. L Zhou, Z Hu, HY Li, J Liu, Y Zeng, et al. (2021) Template-Free Construction of Tin Oxide Porous Hollow Microspheres for Room-Temperature Gas Sensors, ACS Appl. Mater. Interf.

15. H Ding, Y Wei, Z Wu, K Tao, M Ding, X Xie, et al. (2020) Recent Advances in Gas and Humidity Sensors Based on 3D Structured and Porous Graphene and Its Derivatives, ACS Mater Lett 2: 1381-411.

16. U Choi, G Sakai, K Shimanoe, N. Yamazoe, Sensing properties of Au-loaded SnO2–Co3O4 composites to CO and H2, Sens. Actuat. B: Chem 107: 397-401.

17. S Shao, X Chen, Y Chen, L Zhang, H Kim (2020) ACS Appl. ZnO Nanosheets Modified with Graphene Quantum Dots and SnO2 Quantum Nanoparticles for Room-Temperature H2S Sensing, Nano Mater 3: 5220-30.

18. D Degler, U Weimar, N Barsan (2019) Current Understanding of the Fundamental Mechanisms of Doped and Loaded Semiconducting Metal-Oxide-Based Gas Sensing Materials, ACS Sensors 4: 2228-49.

19. P Van, N Thanh, V Quang, N Duy, N Hoa, N Hieu (2014) Scalable Fabrication of High-Performance NO2 Gas Sensors Based on Tungsten Oxide Nanowires by On-Chip Growth and RuO2-Functionalization, ACS Appl. Mater. Interf. 6: 12022-30

20. A Umarji, N Devabharathi, S Dasgupta (2020) Fully Inkjet-Printed Mesoporous SnO2-Based Ultrasensitive Gas Sensors for Trace Amount NO2 Detection, ACS Appl Mater Interf 12: 57207-17.

21. Z Chen, D Pan, Z Li, Z Jiao, M Wu, et al. (2014) Recent Advances in Tin Dioxide Materials: Some Developments in Thin Films, Nanowires, and Nanorods, Chem Rev 114: 7442-86.

22. S Rane, S Arbuj, S Rane, S Gosavi (2015) Hydrogen sensing characteristics of Pt–SnO2nano-structured composite thin films, J. Mat. Sci.: Mater. Electron 26 : 3707-16.

23. FC Chung, RJ Wu, FC Cheng (2014) Fabrication of a Au@SnO2 core–shell structure for gaseous formaldehyde sensing at room temperature, Sens. Actuat B: Chem 190: 1-7.

24. IS Hwang, JK Choi, HS Woo, SJ Kim, SY Jung, et al. (2011) Facilecontrol of C2H5OH sensing characteristics by decorating discrete Ag nanoclusters on SnO2 nanowire networks, ACS Appl. Mater. Interfaces 3: 3140-45.

25. N Ma, K Suematsu, M Yuasa, T Kida, K Shimanoe (2015) Effect of water vapor on Pd-loaded SnO2 nanoparticles gas sensor, ACS Appl. Mater. Interfaces, 7: 5863-9.

26. W Chen, Q Zhou, L Xu, F Wan, S Peng (2013) Improved methane sensing properties of Co-doped SnO2 electrospun nanofibers, J. Nanomater 2013: 173232.

27. KP Gattu, K Ghule, AA Kashale, VB Patil, DM Phase, et al. (2015) Bio-green synthesis of Ni-doped tin oxide nanoparticles and its influence on gas sensing properties, RSC Adv 5: 72849-56.

28. KM Kim, KI Choi, HM Jeong, HJ Kim, HR Kim (2012) Highly sensitive and selective trimethylamine sensors using Ru-doped SnO2 hollow spheres, Sens. Actuat. B: Chem 166: 733-8.

29. YH Cho, X Liang, YC Kang, JH Lee (2015) Ultrasensitive detection of trimethylamine using Rh-doped SnO2 hollow spheres prepared by ultrasonic spray pyrolysis, Sens. Actuat B: Chem 207: 330-37.

30. VM Aroutiounian, VM Arakelyan, MS Aleksanyan, AG Sayunts, GE Shahnazaryan, et al. (2017) Sensor for detection of chemical agents made of Co-doped SnO2, Armenian J Phys 10: 122-7.

31. X Kou, C Wang, M Ding, C Feng, X Li, et al. (2016) Synthesis of Co-doped SnO2 nanofibers and their enhanced gas-sensing properties, Sens. Actuat B: Chem 236: 425.

32. L Liu, C Guo, S Li, L Wang, Q Dong, et al. (2010) Improved H2 sensing properties of Co-doped SnO2 nanofibers, Sens. Actuat B 150: 806-10.

33. K Jain, RP Pant, ST Lakshmikumar (2006) Effect of Ni doping on thick film SnO2 gas sensor, Sens. Actuat. B 113: 823-9.

34. X Liu, J Zhang, X Guo, S Wu, S Wang (2011) Enhanced sensor response of Ni-doped SnO2 hollow spheres, Sens. Actuat. B. 152: 162-7.

35. MM Rahman, A Jamal, SB Khan, M Faisal (2011) Highly sensitive ethanol chemical sensor based on Ni-doped SnO2 nanostructure materials, Biosens. Bioelectr, 28: 127-34.

36. N Tammanoon, A Wisitsoraat, C Sriprachuabwong, D Phokharatkul, A Tuantranont et al. (2015) Ultrasensitive NO2 sensor based on ohmicmetal–semiconductor interfaces of electrolyticallyexfoliatedgraphene/flame-spray-made SnO2 nanoparticles composite operating at low temperatures, ACS Appl Mater Interfaces 7: 24338-52.

37. S Benzitouni, M Zaabat, A Khial, D Rechem, A Benaboud, et al. (2016) High sensitivity of porous Cu-doped SnO2 thin films to methanol, Adv.Nanopart 5: 140-8.

38. N Lavanya, C Sekar, E Fazio, F Neri, SG Leonardi, G Neri (2017) Development of a selective hydrogen leak sensor based on chemically doped SnO2 for automotive applications, Internatl J Hydrogen Energy 42: 10645-55.

39. RN Mariammal, N Rajamanickam, B Renganathan, D Sastikumar, K Ramachandran (2017) Effect of Co on the magnetic and gas sensing properties of SnO2nanoparticles. J Appl Phys 122: 124504,

40. M Punginsang, A Wisitsoraat, C Sriprachuabwong, D Phokharatkul, A Tuantranont, et al. (2016) Roles of cobalt doping on ethanol-sensing mechanisms of flame-spray-made SnO2 nanoparticles–electrolytically exfoliated graphene interfaces, Appl Surf Sci 425: 351-66.

41. Y Tetsunori, M Noritaka, I Masakazu (1991) La2O3-loaded SnO2 Element as a CO2 Gas Sensor 20: 1249-52.

42. H Bai, H Guo, J Wang, Y Dong, B Liu, et al. (2021) Hydrogen gas sensor based on SnO2 nanospheres modified with Sb2O3 prepared by one-step solvothermal route, Sens. Actuat. B: Chem 331: 129441

43. S Singh, R Sattigeri, S Kumar, P Jha, S Sharma (2021) Superior Room-Temperature Ammonia Sensing Using a Hydrothermally Synthesized MoS2/SnO2 Composite, ACS Omega 6: 1602-13.

44. J Bai, C Wang, K Liu, H Wang, Y Liu, et al. (2021) Enhanced gas sensing performance based on the PtCu octahedral alloy nanocrystals decorated SnO2 nanoclusters, Sens. Actuat B: Chem 330: 129375.

45. JM Xu, JP Cheng (2016) The advances of Co3O4 as gas sensing materials: A review, , Journal of Alloys and Compounds 686: 753-68.

46. Lanlan Guo, Fang Chen, Ning Xie, Chong Wang, Xueying Kou, et al. (2018) Metal–organic frameworks derived tin-doped cobalt oxide yolk-shell nanostructures and their gas sensing properties, J Colloid and Interface Science 528: 53–62.

47. CS Jincy, P Meena (2020) Synthesis, characterization, and NH3 gas sensing application of Zn doped cobalt oxide nanoparticles, Inorganic Chemistry Communications 120: 108145.

48. JM Xu, J Zhang, BB Wang, F Liu (2015) Shape-regulated synthesis of cobalt oxide and its gas-sensing property, J Alloys and Compounds 619: 361-7.

49. S Kaciulis, L Pandolfi, E Comini, G Faglia, M Ferroni, et al. (2008) Nanowires of metal oxides for gas sensing applications, Surf. Interface Anal 40: 575-8.

50. W Chen, J Li (2011) Magnetic and electronic structure properties of Co-doped SnO2 nanoparticles synthesized by the sol-gel-

hydrothermal technique. J Appl Phys 109: 083930.

51. B Babu, CV Reddy, J Shim, RVSSN Ravikumar, J Park (2016) Effect of cobalt concentration on morphology of Co-doped SnO2 nanostructures synthesized by solution combustion method, J Mater Sci: Mater Electron 27: 5197–203.

52. LM Fang, XT Zu, ZJ Li, S Zhu, CM Liu, et al. (2008) Microstructure and luminescence properties of Co-doped SnO2 nanoparticles synthesized by hydrothermal method, J Mater Sci: Mater Electron 19: 868-74.

53. J Huang, L Wang, C Gu, M Zhai, J Liu (2013) Preparation of hollow porous Co-doped SnO2microcubes and their enhanced gas sensing property, Cryst Engg. Commun 15: 7515-21.

54. K Srinivas, M Vithal, B Sreedhar, M Manivel Raja, P Venugopal Reddy (2009) Structural, optical, and magnetic properties of nanocrystalline Co doped SnO2based diluted magnetic semiconductors J Phys Chem C 113: 3543-52.

55. Z Song, Z Wei, B Wang, Z Luo, S Xu, et al. (2016) Sensitive room-temperature H2S gas sensors employing SnO2 quantum wire/ reduced graphene oxide nanocomposites. Chem Mater 28: 1205-12.

56. X Liu, N Chen, B Han, X Xiao, G Chen, et al. (2015) Nanoparticle cluster gas sensor: Pt activated SnO2 nanoparticles for NH3 detection with ultrahigh sensitivity, Nanoscale 7: 14872-80.

57. Z Li, Y Dzenis (2011) Highly efficient rapid ethanol sensing based on Co-doped In2O3 nanowires, Talanta. 85: 82-5.

58. L Liu, S Li, J Zhuang, L Wang, J Zhang, et al. (2011) Improved selective acetone sensing properties of Co-doped ZnO nanofibers by electrospinning, Sens. Actuat B 155: 782-8.

59. Z Li, D Ding, Q Liu, C Ning, X Wang (2014) Tuning of structural, optical, and magnetic properties of ultrathin and thin ZnO nanowire arrays for nano device applications, NanoscaleRes Lett 9: 118.

60. M Xu, Q Li, Y Ma, H Fan (2014) Ni-doped ZnO nanorods gas sensor: Enhanced gas-sensing properties, AC and DC electrical behaviors, Sens. Actuat. B Chem 199: 403-9.

61. W Zeng, TM Liu, DJ Liu, EJ Han (2011) Hydrogen sensing and mechanism of M-doped SnO2 (M = Cr3+, Cu2+ and Pd2+) nanocomposite, Sens. Actuat B 160: 455-62.

62. N Barsan, D Koziej, U Weimar (2007) Metal oxide-based gas sensor research: How to?, Sens. Actuat. B: Chem. 121: 18-35.

63. H Windischmann, P Mark (1979) A Model for the operation of a thin-film SnOx conductance-modulation carbon monoxide sensor, J. Electrochem. Soc 126: 627.

64. J Liu, C Wang, Q Yang, Y Gao, X Zhou, et al. (2016) Hydrothermal synthesis and gas-sensing properties of flower-like Sn3O4, Sens. Actuat. B Chem 224: 128-33.

65. H Yamaura, K Moriya, N Miura, N Yamazoe (2000) Mechanism of sensitivity promotion in CO sensor using indium oxide and cobalt oxide, Sens. Actuat. B 64: 39-41.

66. A Sharma, AP Pratap Singh, P Thakur, NB Brookes, S Kumar, et al. (2010) J Appl Phys 107: 093918.

67. M Parthibavarman, B Renganathan, D Sastikumar (2013) Development of high sensitivity ethanol gas sensor based on Co-doped SnO2 nanoparticles by microwave irradiation technique, Current Applied Physics 13: 1537-44.

68. Vertically aligned carbon nanotubes, MoS2–rGo based optoelectronic hybrids for NO2 gas sensing, Foad Ghasemi, Scientific Reports 10: 11306.

69. V Brynzari, G Korotchenkov, S Dmitriev (2000) Theoretical study of semiconductor thin film gas sensitivity: attempt to consistent approach, J. Electron Technol 33: 225–35.

70. G Korotcenkov, I Boris, V Brinzari, SH Han, BK Cho (2013) The role of doping effect on the response of SnO2-based thin film gas sensors: Analysis based on the results obtained for Co-doped SnO2 films deposited by spray pyrolysis, Sens. Actuat B 182: 112–4.